

# The 21cm angular-power spectrum from the dark ages

Antony Lewis<sup>1,\*</sup> and Anthony Challinor<sup>1,2</sup>

<sup>1</sup>*Institute of Astronomy, Madingley Road, Cambridge, CB3 0HA, UK.*

<sup>2</sup>*DAMTP, Centre for Mathematical Sciences, Wilberforce Road, Cambridge CB3 0WA, UK.*

(Dated: December 16, 2018)

At redshifts  $z \gtrsim 30$  neutral hydrogen gas absorbs CMB radiation at the 21cm spin-flip frequency, which is in principle observable and a high-precision probe of cosmology. We calculate the linear-theory angular power spectrum of this signal and cross-correlation between redshifts on all angular scales. In addition to the well known redshift-distortion and density perturbation sources, we also include post-Newtonian corrections and other velocity terms. Although negligible on small scales, these additional terms can be significant at  $l \lesssim 100$  and can be non-zero even when there is no background signal. We also include gravitational lensing and the linear effect of reionization re-scattering, which damps the entire spectrum and also gives a very small polarization signal on large scales.

## I. INTRODUCTION

The cosmic microwave background (CMB) anisotropies have proved to be a valuable source of information about the initial conditions and evolution of the universe. Most current observations measure the CMB temperature and polarization assuming an exactly blackbody spectrum. However by looking at the anisotropies as a function of frequency vastly more information can be obtained. In principle line-absorption from sources along the line of sight to last scattering should be observable (in addition to secondary scattering in clusters). One of the most interesting of these is line absorption due to the 21cm spin-flip transition in neutral hydrogen, giving a low frequency probe of the gas distribution at redshifts  $1000 \gtrsim z \gtrsim 30$  [1, 2, 3]. On small scales the CMB temperature anisotropy is washed out due to photon diffusion damping, limiting the size of perturbations that can be seen directly in the CMB temperature. However the gas distribution is sensitive to all perturbation sizes down to the baryon Jeans' scale, which is orders of magnitude smaller than the photon-damping scale. Hence the 21cm absorption signal probes a much broader range of scales, as well as offering tomographic constraints along the line of sight. Absorption corresponding to an observed wavelength  $\lambda = (1+z)21.106$  cm [ $(1+z)\nu = 1420.4$  MHz] therefore has enormous potential for learning about cosmological perturbations on small scales, as well as new tomographic information about fluctuations on larger scales. Unfortunately observations of the absorption at many-metre wavelengths is very challenging (see e.g. Refs. [3, 4]), but makes a useful target for next-but-one generation experiments.

The origin of the dark-age signal is as follows. For a while after recombination Compton scattering of remaining free electrons with CMB photons keeps the gas temperature coupled to the CMB temperature. However after some expansion the coupling becomes ineffective and the hydrogen gas in the universe starts to cool adiabatically. Atomic collisions in the gas drive the atomic energy levels of the gas towards equilibrium with the gas temperature. The spin temperature measures the relative abundance of triplet and singlet hydrogen states; since the gas cools faster than the CMB, the spin temperature is below the CMB temperature. So at redshifts above  $z \sim 30$  CMB photons will be absorbed by the gas giving an observable 21cm signal from the dark ages. At redshifts  $z \lesssim 30$  atomic collisions become very rare, and the spin temperature is driven back towards the CMB temperature by interaction with the numerous CMB photons: the absorption signal vanishes. At lower redshifts non-linear sources of Lyman- $\alpha$  photons become significant, and again the spin temperature can depart from the CMB temperature, giving a signal in absorption or emission.

In this paper we focus on the absorption signal from  $z \gtrsim 30$  where the physics is well understood and much cleaner than the large uncertainties currently surrounding modelling at lower redshifts. We calculate the linear theory angular power spectrum of the 21cm absorption as a function of redshift, including super-horizon scales where post-Newtonian effects may be important. We focus on the angular power spectrum  $C_l(z, z')$  as this is what is directly observable. Many aspects of the physics may be much clearer with a reconstruction of the 3-D power spectrum [5], but converting the observations into such a spectrum is in general non-trivial especially on large scales, and also dependent on assumptions about the cosmology. Since the perturbations should be accurately linear at high redshifts the statistics should be close to Gaussian, and the angular power spectra should encapsulate all of the statistical information in the

---

\*URL: <http://cosmologist.info>

observation. Our work extends that of Refs. [2, 3, 6, 7, 8, 9] by including linear terms due to gravitational redshifting, all velocity effects, and reionization re-scattering. We find that corrections due to these extra terms are generally small, nonetheless a full calculation and quantification is clearly of interest given the enormous potential of future 21cm observations. Although we do not directly consider  $z \lesssim 30$  here, many of our results could easily be adapted to lower redshifts given a model of the Lyman- $\alpha$  sources and non-linear clustering.

The CMB temperature anisotropy, sourced at  $z \sim 10^3$ , sees super-horizon perturbations at  $l \lesssim 100$ . For a 21cm signal at  $z \sim 50$  the horizon scale is about ten times larger, corresponding to an angular scale  $l \lesssim 10$ . One might therefore expect post-Newtonian effects to dominate at  $l < 10$ . However the small-scale 21cm anisotropy is sourced by spin temperature and redshift distortion fluctuations, which grow rapidly towards smaller scales. The large scale signal is therefore dominated by fluctuations coming from much smaller scales. Since these smaller scales are uncorrelated on large scales, this gives an approximately white-noise 21cm power spectrum on large angular scales. This white-noise signal dominates that from super-horizon scales, so the post-Newtonian corrections are generally below cosmic variance. In addition there are velocity effects, the most important of which is the dipole in the radiation field seen by each hydrogen atom due to its motion with respect to the CMB. This can give non-negligible quantitative corrections to the angular power spectrum at  $l \lesssim 100$ . Re-scattering by the background reionization is small but also induces a small polarization signal. The aim of this paper is to quantify these effects in detail.

The approach we adopt is to evolve the Boltzmann equation for the photon distribution function sourced by absorption of 21cm radiation by neutral hydrogen. We restrict our attention to a spatially-flat close-to-Friedmann-Robertson-Walker cold-dark-matter (CDM) universe. Our results apply equally well with adiabatic or isocurvature scalar mode initial conditions, though we only calculate the adiabatic mode spectra explicitly. We note in passing that 21cm observations are potentially an excellent way to probe isocurvature modes, especially the compensated CDM-baryon mode that cannot be constrained from the CMB temperature [9, 10]. We do not consider the tensor contribution to the intensity power spectrum as the effect is expected to be well below cosmic variance, though we do calculate the tiny tensor-induced polarization signal. We assume no significant particle decay or annihilations, and assume no variation of constants or non-Gaussianity, though these can be well constrained from their effect on the 21cm signal if included [11, 12, 13, 14, 15].

The Boltzmann approach to calculating the line emission angular power spectrum that we consider here is related to the angular power spectrum of source number counts; we discuss this in a companion paper [16].

## II. BOLTZMANN EQUATION

At high redshift perturbations should accurately linear, and we assume there are no sources of Lyman- $\alpha$  photons. During the dark ages the atomic collision time is comparable to the CMB photon interaction time, and for accurate results the full distribution of spin and velocity states must be accounted for [17]. To simplify our analysis we neglect this complication, focussing on the effect of post-Newtonian and bulk velocity effects. We model the spin state distribution by a single spin temperature independent of atomic velocity, with the spin temperature governed by the CMB temperature and collisions. Since the collision rates are not known to better than a couple of percent, and the ionization fraction after recombination is somewhat uncertain, the precision of our calculation is currently limited anyway. We also assume the background CMB temperature is exactly blackbody, neglecting any effects due to distortions, and assume that atomic angular momenta are isotropically distributed.

We employ linearized standard General Relativity, working in the conformal Newtonian gauge with metric

$$ds^2 = a^2(\eta)[(1 + 2\psi)d\eta^2 - (1 - 2\phi)\delta_{ij}dx^i dx^j]. \quad (1)$$

Except when quoting a few results relevant for calculation of numerical answers we use natural units with  $c = 1$ . We take a velocity field  $u^a$  to be along  $\partial_\eta$  so that  $u^\mu = a^{-1}(1 - \psi)\delta_0^\mu$  and  $u_\mu = a(1 + \psi)\delta_{\mu 0}$ . This velocity field is the zeroth element of an orthonormal tetrad which we take to be  $(X_0)^a = u^a$  and  $X_i \equiv a^{-1}(1 + \phi)\partial_i$ . Decomposing a photon wavevector  $k^a = dx^a/d\lambda$  into a direction  $e^a$  and frequency  $k \cdot u \equiv \epsilon/a$ , we have

$$\frac{d\mathbf{x}}{d\eta} = (1 + \phi + \psi)\mathbf{e}, \quad \frac{d\eta}{d\lambda} = a^{-2}\epsilon(1 - \psi), \quad (2)$$

where the three-vector  $\mathbf{e}$  comprises the spatial components of the propagation direction on the spatial triad  $X_i$ .

The number density of neutral hydrogen atoms is  $n_H = n_0 + n_1$ , where the density in the ground state (degeneracy 1) is  $n_0$ , and the density in the upper triplet state (degeneracy 3) is  $n_1$ . We assume the spin temperature  $T_s$  is dependent only on time and position, defined by  $n_1/n_0 = 3e^{-T_\star/T_s}$  where  $T_\star \equiv h_p\nu_{21}/k_B \approx 0.068$  K and  $\nu_{21}$  is the constant 21cm frequency. In the rest frame of the gas the net number of 21cm photons emitted per unit volume in proper time  $d\tau$  within energy  $dE$  is

$$dn_{21} = [(n_1 - 3n_0)B_{10}I_\nu + A_{10}n_1]\delta(E - E_{21})d\tau dE, \quad (3)$$

where  $E_{21}$  corresponds to the 21cm frequency. Here  $A_{10}$  is the spontaneous emission rate, related to the induced rate  $B_{10}$  by detailed balance,  $B_{10} = (\lambda_{21}^3/2h_p c)A_{10}$ . At the temperatures of interest a good approximation for the CMB blackbody brightness is  $I_\nu = 2k_B T_\gamma/\lambda_{21}^2$ . Numerically  $A_{10} = 2\pi\alpha\nu_{21}^3 h_p^2/(3c^4 m_e^2) \approx 2.869 \times 10^{-15} \text{s}^{-1}$  [18], corresponding to a spontaneous decay time of  $\sim 10^7$  years and CMB photon interaction time  $\sim T_*/(T_\gamma A_{10})$  (about  $10^4$  years at  $z = 30$ ). We assume the escape probability is unity: that each line photon does not interact with any more atoms; this is a reasonable approximation since the optical depth to 21cm absorption is only a few percent. We model the source emission as monochromatic, though our results can be integrated over a frequency window function to account for realistic observational bandwidth and intrinsic thermal and quantum line broadening.

Usually the photon temperature  $T_\gamma$  is taken to be isotropic, but here we are interested in corrections and so allow for its angular variation (e.g. due to the dipole in the rest frame of the atom). The gas frame temperature is given by

$$T_\gamma^{(g)}(\mathbf{e}, \mathbf{x}, \eta) = \bar{T}_\gamma(\eta) [1 + \Theta(\mathbf{e}, \mathbf{x}, \eta) - \mathbf{e} \cdot \mathbf{v}(\mathbf{x}, \eta)], \quad (4)$$

where  $\Theta$  is the temperature perturbation and  $\mathbf{v}$  the gas (baryon) velocity relative to  $u^a$  on the  $X_i$  triad. Anisotropy in the radiation field may result in an anisotropic distribution of the atomic triplet states, which would significantly complicate our analysis. This will not be an issue if atomic collisions isotropize the distribution rapidly compared to the photon interaction time. However during the dark ages the collision and photon interaction times are actually similar, so this may not be a safe assumption. Nonetheless, because the interaction is parity invariant, odd multipoles of the radiation field will not affect the triplet distribution; in particular the dominant dipole term leaves an isotropic distribution unchanged. Higher order CMB anisotropies will drive an anisotropy in the triplet distribution, however their relative amplitude is  $\sim 10^{-4}$  so their contribution is very small. Also the scattering time for a photon from the anisotropic part of the distribution will be longer than the collision time, so the distribution should in any case be randomized effectively. Similar comments apply to the effect of polarized radiation, so our approximation of an isotropic triplet distribution should be accurate.

If the gas 4-velocity is  $u_g^a$  the rest frame energy is given by  $E^{(g)} = k_a u_g^a = \epsilon(1 - \mathbf{e} \cdot \mathbf{v})/a$ , and an interval  $d\lambda$  along the photon path corresponds to a proper time  $d\tau = u_g^a dx_a = k_a u_g^a d\lambda$ . The Boltzmann equation for the evolution of the distribution function  $f$  (number density of photons  $dn_{21} = f d\Omega E^2 dE$ ) is then

$$\begin{aligned} \left. \frac{df}{d\lambda} \right|_H &= \frac{E_{21}}{4\pi E_{21}^2} \frac{3n_H A_{10}}{3 + e^{T_*/T_s}} \left[ (1 - e^{T_*/T_s}) \frac{T_\gamma^{(g)}}{T_*} + 1 \right] \delta(k_a u_g^a - E_{21}) \\ &\approx \frac{1}{4\pi E_{21}} \frac{3\bar{n}_H A_{10}}{4} \left[ 1 + \Delta_H - \frac{\bar{T}_\gamma(1 + \Theta - \mathbf{e} \cdot \mathbf{v} - \Delta_{T_s})}{\bar{T}_s} \right] \delta(\epsilon(1 - \mathbf{e} \cdot \mathbf{v})/a - E_{21}), \end{aligned} \quad (5)$$

where  $n_H$  is the number density of neutral hydrogen and we used the good approximation  $T_* \ll T_s$ . We defined fractional perturbations in a quantity  $X$  as  $\Delta_X \equiv (\delta X)/\bar{X}$  and denoted background quantities by an overbar. Since the baryon pressure is very low we may take  $\Delta_H = \Delta_b$ , though the baryon perturbation  $\Delta_b$  can differ significantly from the CDM perturbation  $\Delta_c$ . Defining

$$\bar{\rho}_s \equiv \frac{1}{4\pi E_{21}^2} \frac{3\bar{n}_H A_{10}}{4} \left( \frac{\bar{T}_s - \bar{T}_\gamma}{\bar{T}_s} \right), \quad (6)$$

the monopole perturbation source is

$$\Delta_s \equiv \Delta_H + \frac{\bar{T}_\gamma}{\bar{T}_s - \bar{T}_\gamma} (\Delta_{T_s} - \Delta_{T_\gamma}) \quad (7)$$

and the Boltzmann equation becomes

$$\left. \frac{df}{d\lambda} \right|_H = E_{21} \bar{\rho}_s \left[ 1 + \Delta_s - \frac{\bar{T}_\gamma}{\bar{T}_s - \bar{T}_\gamma} \{ \mathbf{e} \cdot (\mathbf{v}_\gamma - \mathbf{v}) + \Theta_+ \} \right] \delta(\epsilon(1 - \mathbf{e} \cdot \mathbf{v})/a - E_{21}). \quad (8)$$

Here  $\Theta_+$  denotes the gauge-invariant temperature anisotropy sources with  $l \geq 2$ , and  $\mathbf{v}_\gamma$  is the velocity (i.e. dipole) of the photon distribution.

Although we do not model reionization in detail here, we do include re-scattering by the background electron density as this affects the power spectrum seem from the dark ages. For the moment we neglect polarization and discuss this later. The Thomson scattering contribution to the Boltzmann equation is then

$$\begin{aligned} \left. \frac{df}{d\lambda} \right|_{\text{Thomson}} &= E^{(g)} n_e \sigma_T \left[ \frac{3}{16\pi} \int d\tilde{\Omega}_{\tilde{\mathbf{e}}'} \tilde{f}(E^{(g)}, \tilde{\mathbf{e}}') [1 + (\tilde{\mathbf{e}} \cdot \tilde{\mathbf{e}}')^2] - f(E, \mathbf{e}) \right] \\ &\approx E^{(g)} n_e \sigma_T \left[ \frac{3}{16\pi} \int d\Omega_{\mathbf{e}'} f(E, \mathbf{e}') [1 + (\mathbf{e} \cdot \mathbf{e}')^2] - \mathbf{e} \cdot \mathbf{v} \epsilon \partial_\epsilon \bar{f} - f(E, \mathbf{e}) \right]. \end{aligned} \quad (9)$$

In the first line here, the tildes denote quantities in the gas frame evaluated on the Lorentz-boosted tetrad  $\tilde{X}_\mu$ . Performing the remaining angular integral, the total Boltzmann equation for the change in the distribution function due to 21cm absorption and 21cm re-scattering becomes

$$\frac{df}{d\lambda} = E_{21}\bar{\rho}_s \left[ 1 + \Delta_s - \frac{\bar{T}_\gamma}{T_s - \bar{T}_\gamma} \{ \mathbf{e} \cdot (\mathbf{v}_\gamma - \mathbf{v}) + \Theta_+ \} \right] \delta(\epsilon(1 - \mathbf{e} \cdot \mathbf{v})/a - E_{21}) + \frac{\epsilon\bar{n}_e\sigma_T}{a} \left[ F - \epsilon\partial_\epsilon\bar{f}\mathbf{e} \cdot \mathbf{v} + \frac{f_2}{10} - f \right], \quad (10)$$

where  $F$  and  $f_2$  are the monopole and quadrupole parts of  $f$ .

Denoting background quantities with an overbar, the background equation is

$$\frac{\partial\bar{f}}{\partial\eta} = a\bar{\rho}_s\delta(\epsilon/a - E_{21}), \quad (11)$$

which integrates to

$$\bar{f}(\eta, \epsilon) = \left[ \frac{a\bar{\rho}_s}{E_{21}\mathcal{H}} \right]_\epsilon \theta(\eta - \eta_\epsilon) \equiv \bar{f}(\epsilon)\theta(\eta - \eta_\epsilon). \quad (12)$$

Here a subscript  $\epsilon$  denotes the quantity is evaluated at time  $\eta_\epsilon$  [and additionally position  $\mathbf{x}_A + \hat{\mathbf{n}}(\eta_A - \eta_\epsilon)$  for perturbed quantities along a line of sight  $\hat{\mathbf{n}}$ ], where  $\epsilon = a(\eta_\epsilon)E_{21}$ ,  $\theta(x)$  is the Heaviside function,  $A$  denotes the observation point and  $\mathcal{H}$  is the conformal Hubble parameter. The brightness temperature observed today is given by  $T_b = \lambda_{\text{obs}}^2 I_\nu / 2k_B$  and  $I_\nu = E_{\text{obs}}^3 h_p f / c^2$ , with the result that the isotropic brightness today due to background emission is

$$\bar{T}_b(\epsilon) = \left[ \frac{3\lambda_{21}^2 h_p c A_{10} \bar{n}_H (\bar{T}_s - \bar{T}_\gamma)}{32\pi k_B \bar{T}_s H} \frac{(\bar{T}_s - \bar{T}_\gamma)}{1+z} \right]_\epsilon \equiv \tau_{21}(\epsilon) \frac{(\bar{T}_s - \bar{T}_\gamma)}{1+z} \Big|_\epsilon. \quad (13)$$

Here  $\tau_{21}(\epsilon)$  defines the optical depth to 21cm absorption, which is typically 2–3%. During the dark ages the spin temperature is below the CMB temperature, so  $\bar{T}_b$  is negative corresponding to net absorption.

To solve the perturbed Boltzmann equation we use the time component of the geodesic equation, which reduces to an equation for the evolution of the comoving energy along the line of sight:

$$\frac{d\epsilon}{d\eta} = -\epsilon \frac{d\psi}{d\eta} + \epsilon(\dot{\phi} + \dot{\psi}), \quad (14)$$

where overdots denote conformal time partial derivatives. We parameterize the distribution function in the Newtonian gauge as  $f(\eta, \mathbf{x}, \epsilon, \mathbf{e})$ , in which case the Boltzmann equation becomes

$$\frac{\partial f}{\partial\eta} + \mathbf{e} \cdot \nabla f + \epsilon\partial_\epsilon\bar{f} \left( \dot{\phi} + \dot{\psi} - \frac{d\psi}{d\eta} \right) = a\bar{\rho}_s \left[ 1 + \Delta_s + \psi - \mathbf{e} \cdot \mathbf{v} - \frac{\bar{T}_\gamma}{T_s - \bar{T}_\gamma} \{ \mathbf{e} \cdot (\mathbf{v}_\gamma - \mathbf{v}) + \Theta_+ \} \right] \delta(\epsilon/a - E_{21}) - a\bar{\rho}_s \mathbf{e} \cdot \mathbf{v} \epsilon \partial_\epsilon \delta(\epsilon/a - E_{21}) + a\bar{n}_e \sigma_T \left[ F - \epsilon\partial_\epsilon\bar{f}\mathbf{e} \cdot \mathbf{v} + \frac{f_2}{10} - f \right]. \quad (15)$$

Noting that  $\epsilon\partial_\epsilon = \mathcal{H}_\epsilon^{-1}\partial_{\eta_\epsilon}$ , we have

$$\begin{aligned} \epsilon\partial_\epsilon\bar{f}(\eta, \epsilon) &= \frac{1}{\mathcal{H}_\epsilon} \left[ \frac{\partial}{\partial\eta} \left( \frac{a\bar{\rho}_s}{E_{21}\mathcal{H}} \right) \right]_\epsilon \theta(\eta - \eta_\epsilon) - \left( \frac{a\bar{\rho}_s}{E_{21}\mathcal{H}^2} \right)_\epsilon \delta(\eta - \eta_\epsilon) \\ &= \bar{f}_{,\ln\epsilon}(\epsilon)\theta(\eta - \eta_\epsilon) - \frac{\bar{f}(\epsilon)}{\mathcal{H}_\epsilon} \delta(\eta - \eta_\epsilon), \end{aligned} \quad (16)$$

which defines an additional time-independent quantity  $\bar{f}_{,\ln\epsilon}(\epsilon)$ . Substituting into the Boltzmann equation and integrate formally along the background line of sight gives the final result

$$\begin{aligned} \delta f(\eta_A, \mathbf{x}_A, \epsilon, \hat{\mathbf{n}}) &= e^{-\tau_\epsilon} \bar{f}(\epsilon) \left[ \Delta_s + \psi + \hat{\mathbf{n}} \cdot \mathbf{v} + \frac{\bar{T}_\gamma}{T_s - \bar{T}_\gamma} \{ \hat{\mathbf{n}} \cdot (\mathbf{v}_\gamma - \mathbf{v}) - \Theta_+ \} + \frac{1}{\mathcal{H}} \left( -\frac{d\psi}{d\eta} + (\dot{\phi} + \dot{\psi}) + \hat{\mathbf{n}} \cdot \frac{d\mathbf{v}}{d\eta} \right) \right]_\epsilon \\ &+ e^{-\tau_\epsilon} \bar{f}_{,\ln\epsilon}(\epsilon) (e^{\tau_\epsilon} \psi_A - \psi_\epsilon + \hat{\mathbf{n}} \cdot \mathbf{v}_\epsilon) - \bar{f}_{,\ln\epsilon}(\epsilon) \int_{\eta_\epsilon}^{\eta_A} d\eta e^{-\tau} (\dot{\phi} + \dot{\psi}) - \int_{\eta_\epsilon}^{\eta_A} d\eta \dot{\tau} e^{-\tau} \left( \delta f_0 + \bar{f}_{,\ln\epsilon}(\epsilon) (\hat{\mathbf{n}} \cdot \mathbf{v} - \psi) + \frac{f_2}{10} \right), \end{aligned} \quad (17)$$

where  $\tau$  is the Thomson scattering optical depth,  $\hat{\mathbf{n}} = -\mathbf{e}|_A$  and  $\epsilon < a_A E_{21}$  (i.e. observed energy strictly less than  $E_{21}$ ), and  $\delta f_0$  is the monopole perturbation. We have assumed that the CMB anisotropies can be well observed at higher frequencies, and the first-order perturbation from last scattering subtracted off the 21cm map. The 21cm brightness fluctuation calculated here is then that of the difference map without the blackbody contribution.

The first term in Eq. (17) is the usual monopole source, with additional terms  $\psi + \hat{\mathbf{n}} \cdot \mathbf{v}$  reflecting the additional emission due to the difference between proper time in the gas frame and the interval  $d\eta$  along the line of sight. Then there is the effect from the CMB dipole seen in the gas frame,  $\mathbf{v}_\gamma - \mathbf{v}$ , plus higher multipole contributions to the temperature seen by the source,  $\Theta_+$ . The remaining terms on the first line of Eq. (17) describe the local effect of gravitational and Doppler redshifting on the relation between an observed redshift interval  $\Delta z$  and the  $\Delta\eta$  along the line of sight. The main such redshift-distortion effect comes from the radial gradient contribution to  $\hat{\mathbf{n}} \cdot (d\mathbf{v}/d\eta)$ . The term multiplying  $\bar{f}_{,\ln\epsilon}(\epsilon)$  is just  $\mathcal{H}\delta\eta$  where  $\delta\eta$  is the perturbation to the conformal time for a fixed (gas-frame) redshift surface; it has the usual Doppler, Sachs-Wolfe and integrated Sachs-Wolfe contributions familiar from CMB studies.

To understand the way in which reionization enters Eq. (17), consider reionization approximated by a delta-function visibility function at time  $\eta_{\text{re}}$  with optical depth  $\tau$ . We then have

$$\begin{aligned} \delta f(\eta_A, \mathbf{x}_A, \epsilon, \hat{\mathbf{n}}) = & \\ & e^{-\tau} \bar{f}(\epsilon) \left[ \Delta_s + \psi + \hat{\mathbf{n}} \cdot \mathbf{v} + \frac{\bar{T}_\gamma}{T_s - \bar{T}_\gamma} \{ \hat{\mathbf{n}} \cdot (\mathbf{v}_\gamma - \mathbf{v}) - \Theta_+ \} + \frac{1}{\mathcal{H}} \left( -\frac{d\psi}{d\eta} + (\dot{\phi} + \dot{\psi}) + \hat{\mathbf{n}} \cdot \frac{d\mathbf{v}}{d\eta} \right) \right]_\epsilon \\ & + e^{-\tau} \bar{f}_{,\ln\epsilon}(\epsilon) \left( \psi_A - \psi_\epsilon + \hat{\mathbf{n}} \cdot \mathbf{v}_\epsilon - \int_{\eta_\epsilon}^{\eta_A} d\eta (\dot{\phi} + \dot{\psi}) \right) + (1 - e^{-\tau}) \bar{f}_{,\ln\epsilon}(\epsilon) \left( \psi_A - \psi_{\text{re}} + \hat{\mathbf{n}} \cdot \mathbf{v}_{\text{re}} - \int_{\eta_{\text{re}}}^{\eta_A} d\eta (\dot{\phi} + \dot{\psi}) \right) \\ & + (1 - e^{-\tau}) \left( \delta f_0(\epsilon) + \frac{1}{10} f_2(\epsilon, \mathbf{e}) \right)_{\text{re}}. \quad (18) \end{aligned}$$

The first two sets of terms are the  $\delta f$  without reionization multiplied by the fraction,  $e^{-\tau}$ , of 21cm photons that are not rescattered. The third set contains the effective  $\delta\eta$  for those photons that do rescatter (i.e. only the common part that is accrued after reionization) weighted by the fraction,  $1 - e^{-\tau}$ , that scatter. Finally, the fourth terms arise from in-scattering at reionization and represents an average of the source functions on the electrons' 21cm surface. For perturbation modes with  $k(\eta_{\text{re}} - \eta_\epsilon) \gg 1$ , the dominant contribution to the 21cm monopole at reionization is  $\delta f_0(\epsilon)|_{\text{re}} \approx \bar{f}_{,\ln\epsilon}(\epsilon)\psi|_{\text{re}}$  since the source terms on the electrons' 21cm surface average to zero. Using this in Eq. (18), we see that for such modes reionization damps the 21cm anisotropies by  $e^{-\tau}$ . For modes with  $k(\eta_{\text{re}} - \eta_\epsilon) \ll 1$ , reionization has essentially no effect since scattering out of the line of sight is balanced by in-scattering. However, the contribution from such modes (which were necessarily outside the horizon at  $\eta_\epsilon$ ) to the 21cm anisotropy at any multipole  $l$  is now small since there is considerably more power in modes with larger  $k$  (see Sec. V). The net effect is that reionization should suppress the 21cm anisotropies by  $e^{-\tau}$  on all scales, unlike the CMB where there is no suppression at large  $l$ .

On small scales most of the terms are completely negligible, and the result is accurately given by the standard approximation

$$\delta f(\eta_A, \mathbf{x}_A, \epsilon, \hat{\mathbf{n}}) \approx e^{-\tau} \bar{f}(\epsilon) \left[ \Delta_s - \frac{1}{\mathcal{H}} \hat{\mathbf{n}} \cdot \frac{\partial \mathbf{v}}{\partial \chi} \right]_\epsilon, \quad (19)$$

where  $\chi \equiv \eta_A - \eta$  is the conformal distance along the line of sight. To consider the impact of the additional terms on large scales we next derive an expression for the power spectrum for numerical calculation.

### III. ANGULAR POWER SPECTRUM

For numerical work one can expand into multipoles and harmonics. We use

$$\begin{aligned} \delta f(\eta, \mathbf{x}, \epsilon, \mathbf{e}) &= \sum_{l \geq 0} \int \frac{d^3 \mathbf{k}}{(2\pi)^{3/2}} (-i)^l (2l+1) F_l(\eta, \epsilon, \mathbf{k}) P_l(\hat{\mathbf{k}} \cdot \mathbf{e}) e^{i\mathbf{k} \cdot \mathbf{x}} \\ &= 4\pi \sum_{lm} \int \frac{d^3 \mathbf{k}}{(2\pi)^{3/2}} (-i)^l F_l(\eta, \epsilon, \mathbf{k}) Y_{lm}^*(\hat{\mathbf{k}}) Y_{lm}(\mathbf{e}) e^{i\mathbf{k} \cdot \mathbf{x}}, \quad (20) \end{aligned}$$

$$\mathbf{v}_i(\eta, \mathbf{x}) = \int \frac{d^3 \mathbf{k}}{(2\pi)^{3/2}} (-i) v_i(\eta, \mathbf{k}) \hat{\mathbf{k}} e^{i\mathbf{k} \cdot \mathbf{x}}, \quad (21)$$

for the  $i$ th species, and similarly for the temperature multipoles, giving

$$\begin{aligned}
F_l(\eta_A, \epsilon, \mathbf{k}) = & e^{-\tau_\epsilon} \left\{ \bar{f}(\epsilon) \left[ \Delta_s + \psi + \frac{\dot{\phi}}{\mathcal{H}} \right]_\epsilon - \bar{f}_{,\ln\epsilon}(\epsilon) \psi_\epsilon \right\} j_l(k\chi_\epsilon) - \bar{f}_{,\ln\epsilon}(\epsilon) \int_{\eta_\epsilon}^{\eta_A} d\eta e^{-\tau} (\dot{\phi} + \dot{\psi}) j_l(k\chi) \\
& - e^{-\tau_\epsilon} \left[ \frac{\bar{f}(\epsilon)}{\mathcal{H}} (\dot{v} + \mathcal{H}v - k\psi) + \bar{f}_{,\ln\epsilon}(\epsilon) v + \bar{f}(\epsilon) \frac{\bar{T}_\gamma}{\bar{T}_s - \bar{T}_\gamma} (v_\gamma - v) \right]_\epsilon j'_l(k\chi_\epsilon) + e^{-\tau_\epsilon} \bar{f}(\epsilon) \frac{kv}{\mathcal{H}} j''_l(k\chi_\epsilon) \\
& - \int_{\eta_\epsilon}^{\eta_A} d\eta \dot{\tau} e^{-\tau} \left[ (F_0 - \bar{f}_{,\ln\epsilon}(\epsilon) \psi) j_l(k\chi) - \bar{f}_{,\ln\epsilon}(\epsilon) v j'_l(k\chi) + \frac{F_2}{4} \{3j''_l(k\chi) + j_l(k\chi)\} \right] \\
& - e^{-\tau_\epsilon} \bar{f}(\epsilon) \frac{\bar{T}_\gamma}{\bar{T}_s - \bar{T}_\gamma} \sum_{l'=2}^{\infty} (2l' + 1) \Theta_{l'l} i^{l'} P_{l'} \left( -\frac{i}{k} \frac{d}{d\chi_\epsilon} \right) j_l(k\chi_\epsilon) \quad (22)
\end{aligned}$$

for  $l \geq 1$ , where a prime denotes a derivative with respect to the argument. The last term is small, of the order of the  $l \geq 2$  CMB temperature fluctuation. Note that  $\dot{v} + \mathcal{H}v - k\psi$  is zero in the absence of Thomson scattering or baryon pressure effects. Equation (22) can be integrated over a given frequency window function (determined by the observation) to determine the actual observed power. If desired one can integrate by parts so that the result depends only on  $j_l$  and derivatives of the window function and sources. We perform our numerical calculations this way in the synchronous gauge: the equations in a general gauge are give in Appendix B.

The angular power spectrum is given by

$$C_l(z, z') = 4\pi \int d \ln k \mathcal{P}_\chi(k) F_l(k, z) F_l(k, z'), \quad (23)$$

where  $\mathcal{P}_\chi$  is the power spectrum of the primordial curvature perturbation  $\chi$  and  $F_l(k, z)$  is the distribution function multipole transfer function to redshift  $z = a_A E_{21}/\epsilon - 1$ ; i.e.  $F_l(k, z) = F_l(\eta_A, E_{21}/(1+z), \mathbf{k})$  for unit initial curvature perturbation.

To calculate the sources for the line-of-sight integral we need to compute the perturbations in the spin and gas temperatures, and, for reionization, the evolution of the low multipoles of the distribution function. We consider these next.

#### IV. PERTURBATION EVOLUTION

The evolution of the spin temperature is determined from the evolution equation for the states of a fixed number of atoms  $N_H = N_0 + N_1$  in the gas rest frame. If we crudely assume that recombinations are to the singlet and triplet state in the ratio 1:3 we have

$$\frac{\partial N_0}{\partial \tau} = -N_0(C_{01} + B_{01}I_{\nu 0}) + N_1(C_{10} + A_{10} + B_{10}I_{\nu 0}) - \frac{\partial x_e}{\partial \tau} \frac{N_H + N_e}{4}, \quad (24)$$

where  $\tau$  is the gas proper time,  $I_{\nu 0}$  is the monopole part of  $I_\nu$  in the gas frame, and the ionization fraction is  $x_e \equiv n_e/(n_H + n_p)$  (we are neglecting molecular hydrogen and assume all helium is neutral). Here  $B_{01} = 3B_{10}$  and the collision term is  $C_{10} = \kappa_{10}^{HH} n_H + \kappa_{10}^{eH} n_e + \kappa_{10}^{pH} n_p$  and  $C_{01} = 3C_{10} e^{-T_\star/T_g}$  where  $T_g$  is the gas temperature. The rates  $\kappa_{10}^i$  for hydrogen-hydrogen, hydrogen-electron and hydrogen-proton collisional coupling are taken from Refs. [3, 19] (fit using a cubic splines and 5th order polynomial in the logs), and not known to an accuracy of better than a few percent. As shown in Fig. 1 the hydrogen-hydrogen term dominates because of the small dark-age ionization fraction ( $x_e \sim 2 \times 10^{-4}$ ), and proton-hydrogen rates are suppressed relative to electron-hydrogen rates by a factor of  $\sim (m_e/m_p)^{1/2}$  due to the lower proton velocity, except at low redshifts where the proton cross-section is significantly higher [19]. We include the small correction from electron-hydrogen collisions, but neglect the proton-hydrogen term. At redshift  $z \sim 70$  the total collisional and photon interaction rates are about equal,  $C_{10} \sim T_\gamma A_{10}/T_\star$ , with  $C_{10} \sim 10^{-11} \text{s}^{-1}$  (corresponding to a collisional coupling time  $\sim 4000$  years). At lower redshifts the gas becomes diffuse and collisions become less effective at coupling the spin temperature to the gas temperature. Defining  $\beta_s \equiv 1/T_s$  (etc.), the evolution of the spin temperature is determined by

$$\frac{\partial \beta_s}{\partial \tau} + \frac{\beta_s}{1 - x_e} \frac{\partial x_e}{\partial \tau} = 4 \left[ (\beta_g - \beta_s) C_{10} + \frac{\beta_\star}{\beta_\gamma} (\beta_\gamma - \beta_s) A_{10} \right]. \quad (25)$$

In the epoch before reionization the spin temperature and ionization fraction only vary on Hubble time scales. The coupling time is short compared to the Hubble time, so the spin temperature is determined to good accuracy by

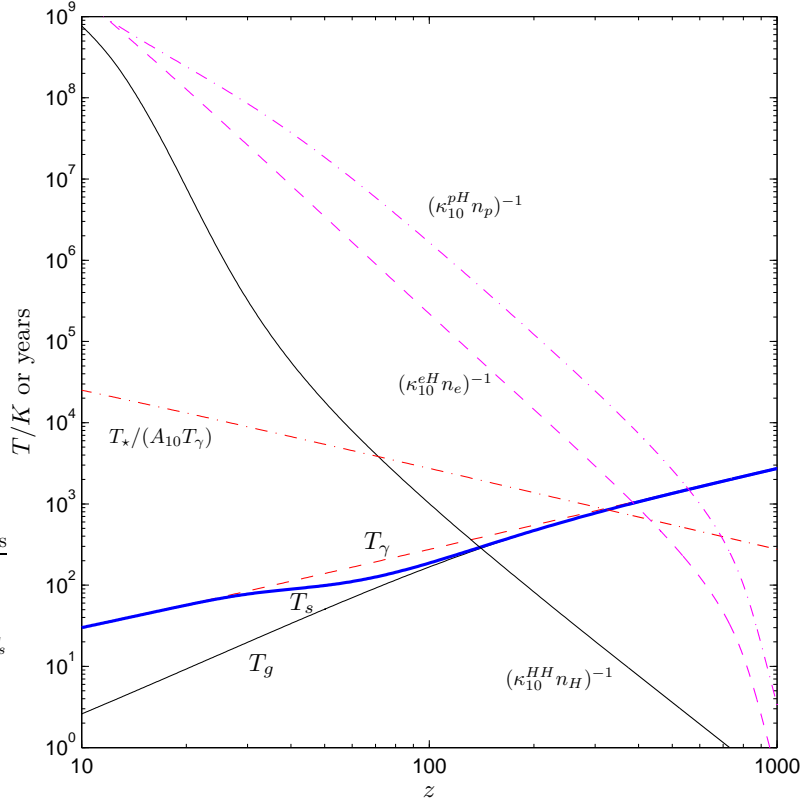


FIG. 1: Evolution of the interaction times for H-H, H-e, H-p and H-photon spin-coupling processes, and how this influences the spin temperature  $T_s$  relative to the background CMB and gas temperatures. At high temperatures the H-H collision time is short and collisions couple  $T_s$  to the gas temperature  $T_g$ ; at lower redshifts the gas is diffuse and CMB photon interactions drive  $T_s$  to the CMB temperature  $T_\gamma$ . This figure assumes purely linear evolution and no Lyman-alpha coupling; in reality non-linear sources are likely to change the result at  $z \lesssim 30$ .

equilibrium, with the left hand side of Eq. (25) being zero,

$$T_s = T_\gamma \left( \frac{C_{10}/T_\gamma + A_{10}/T_\star}{C_{10}/T_g + A_{10}/T_\star} \right), \quad (26)$$

which varies between  $T_\gamma$  and  $T_g$  depending on whether the radiation or collision terms dominate; see Fig. 1.

This equation is frame invariant, and the gauge-invariant equation for the (gauge-dependent) perturbations is

$$\begin{aligned} \Delta_{T_s} - \Delta_{T_\gamma} &= (R_\gamma - R_g)C_{10}\Delta C_{10} + C_{10}(R_g\Delta T_g - R_\gamma\Delta T_\gamma) \\ &= \left( \Delta_H C_{10} + \left[ \frac{d \ln \kappa_{10}^{HH}}{d \ln T_g} \bar{n}_H \kappa_{10}^{HH} + \frac{d \ln \kappa_{10}^{eH}}{d \ln T_g} \bar{n}_e \kappa_{10}^{eH} \right] \Delta T_g \right) (R_\gamma - R_g) + C_{10}(R_g\Delta T_g - R_\gamma\Delta T_\gamma), \end{aligned} \quad (27)$$

where  $R_i^{-1} \equiv (C_{10} + A_{10}\bar{T}_i/T_\star)$  and we neglect terms in  $\Delta_{x_e}$ , the perturbation to the ionization fraction. The background ionization fraction is taken from RECFAST [20].

Assuming purely Compton cooling, the background gas temperature evolves according to [20, 21]

$$\dot{\bar{T}}_g + 2\mathcal{H}\bar{T}_g = -\frac{8a\sigma_T\bar{\rho}_\gamma x_e}{3m_e c(1 + f_{\text{He}} + x_e)} (\bar{T}_g - \bar{T}_\gamma), \quad (28)$$

where  $\sigma_T$  is the Thomson scattering cross-section and  $f_{\text{He}} = n_{\text{He}}/(n_{\text{H}} + n_{\text{p}})$ . The perturbations evolve with

$$\dot{\Delta}_{T_g} = 2\dot{\phi} - \frac{2}{3}kv - \frac{8a\sigma_T\bar{\rho}_\gamma x_e}{3m_e c(1 + f_{\text{He}} + x_e)} \left[ \left( 1 - \frac{\bar{T}_\gamma}{\bar{T}_g} \right) (4\Delta_{T_\gamma} + \psi) + \frac{\bar{T}_\gamma}{\bar{T}_g} (\Delta_{T_g} - \Delta_{T_\gamma}) \right], \quad (29)$$

where we again neglected  $\Delta_{x_e}$  (and helium fraction perturbations). Typical transfer functions for the perturbations are shown in Fig. 3 *in the synchronous gauge* that we use for numerical work. The Newtonian-gauge functions differ

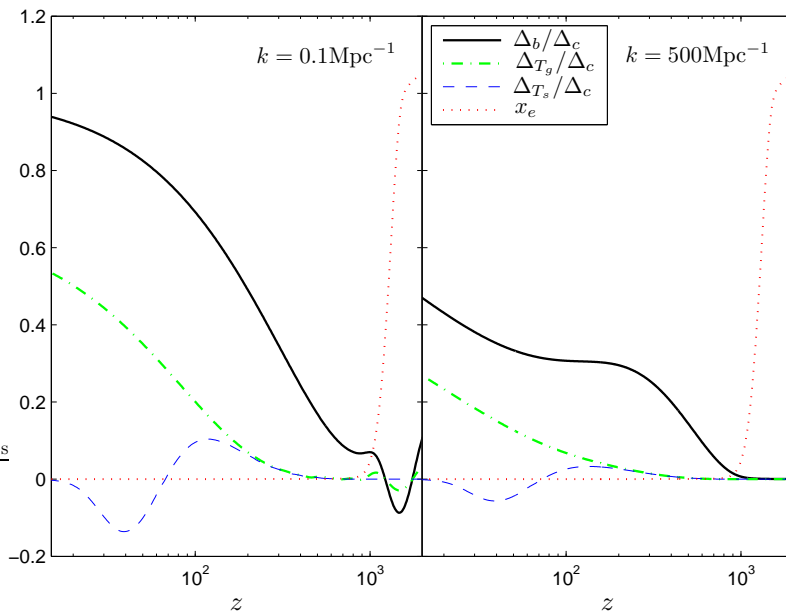


FIG. 2: Evolution of the fractional baryon, matter and spin temperature perturbations as a fraction of the CDM density perturbation. The left figure is for a  $k = 0.1 \text{Mpc}^{-1}$  mode, the right figure shows the effect of baryon pressure at  $k = 500 \text{Mpc}^{-1}$ . In both cases the baryon perturbation is significantly less than the CDM perturbation at all relevant redshifts. There is no reionization.

on super-horizon scales ( $k \lesssim 10^{-3} \text{Mpc}^{-1}$  at  $z = 50$ ). For example, the CDM transfer function flattens to  $\approx 6/5$  on large scales.

Assuming an ideal gas, the gas pressure perturbation  $\delta p/\bar{\rho}_g = c_s^2 \Delta_g$  is given by

$$c_s^2 \Delta_g = \frac{k_B \bar{T}_g}{\mu} (\Delta_g + \Delta_{T_g}) \approx \frac{k_B \bar{T}_g}{m_p} ([1 + x_e](1 - Y_{\text{He}}) + Y_{\text{He}} m_p/m_{\text{He}}) (\Delta_g + \Delta_{T_g}), \quad (30)$$

where  $\mu$  is the mean particle mass and  $Y_{\text{He}}$  is the mass fraction in helium. This result must be used on scales where the baryon pressure is important [8]. Note that on these scales there may also be additional effects due to CDM decoupling [22] that we neglect here. The evolution of the gas and spin temperature perturbations is shown in Figure 2 for two different scales, along with the relative evolution of the baryon and CDM perturbations. Again, these are in the synchronous gauge but they are very similar to the Newtonian-gauge perturbations since both wavelengths are sub-horizon for the redshift range plotted.

To evaluate the sources for reionization Thomson scattering we need to evolve the multipole equation

$$\begin{aligned} \dot{F}_l + \frac{k}{2l+1} [(l+1)F_{l+1} - lF_{l-1}] + \delta_{l0} \epsilon \partial_\epsilon \bar{f} \dot{\phi} + \frac{\delta_{l1}}{3} \epsilon \partial_\epsilon \bar{f} k \psi = \\ a \bar{\rho}_s \left[ \delta_{l0} (\Delta_s + \psi) - \frac{\delta_{l1}}{3} \left( v + \frac{\bar{T}_\gamma}{\bar{T}_s - \bar{T}_\gamma} (v_\gamma - v) \right) - (1 - \delta_{l0} - \delta_{l1}) \frac{\bar{T}_\gamma}{\bar{T}_s - \bar{T}_\gamma} \Theta_l \right] \delta(\epsilon/a - E_{21}) \\ - \delta_{l1} a \bar{\rho}_s \frac{v}{3} \epsilon \partial_\epsilon \delta(\epsilon/a - E_{21}) - \dot{\tau} \left[ (\delta_{l0} - 1) F_l - \frac{\delta_{l1}}{3} v \epsilon \partial_\epsilon \bar{f} + \delta_{l2} \frac{F_2}{10} \right]. \quad (31) \end{aligned}$$

Integration over a window function in frequency removes the delta-functions so the equation for the energy integrated multipoles can easily be integrated numerically, as discussed further in Appendix B. Other perturbed quantities and the photon temperature and polarization multipoles evolve according to standard results as implemented in the numerical codes CMBFAST and CAMB [23, 24, 25, 26].

## V. APPROXIMATE RESULTS

The general form of the equal-redshift angular power spectra can easily be understood. On super-horizon scales the potential  $\phi$  is close to scale invariant and constant, so (from the Poisson equation in the comoving gauge)

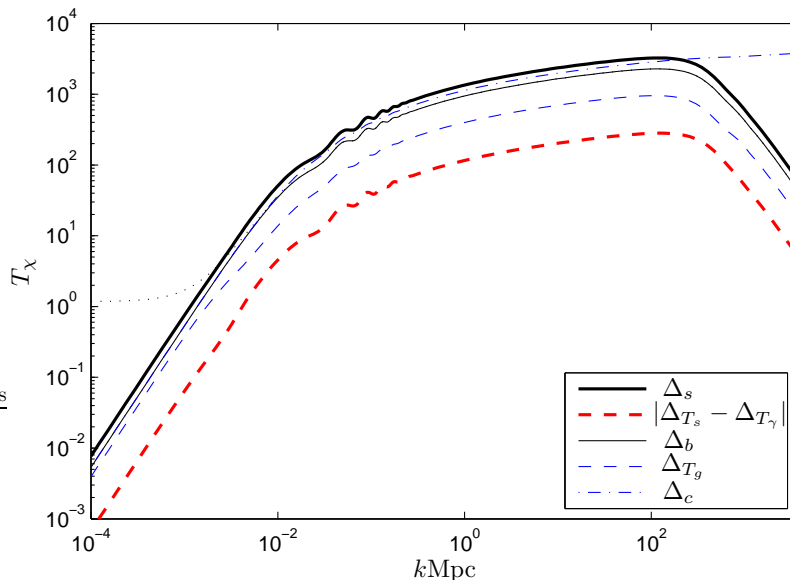


FIG. 3: Transfer function for monopole source at redshift  $z = 50$  given unit initial curvature perturbation, compared to other relevant perturbations. The perturbations are numerically evaluated in the synchronous gauge. The Newtonian-gauge fluctuations equal those in the synchronous gauge well inside the horizon ( $k \gg 10^{-3} \text{ Mpc}^{-1}$ ). On large scales, the Newtonian-gauge  $\Delta_b$  flattens out at  $\approx 6/5$  times the primordial curvature perturbation, as shown by the dotted curve. The spin temperature perturbation is negative at  $z = 50$  (see Fig. 2).

$\Delta_c \sim k^2/\mathcal{H}^2\phi$ . Hence on entering the horizon the matter perturbations have  $\Delta_c \sim \phi$ . During radiation domination photon pressure prevents gravitational collapse: the perturbations only grow logarithmically. As a result the spectrum of  $\Delta_c$  is approximately scale invariant on sub-horizon scales at matter-radiation equality, though super-horizon scales still have  $\Delta_c \sim k^2/\mathcal{H}^2\phi$ . During matter domination the potential remains constant and  $\Delta_c$  grows at the same rate independent of  $k$  on all scales where baryon pressure can be neglected. The result is that an initially scale-invariant potential gives comoving-gauge CDM perturbations with an amplitude scaling as  $k^2$  on large scales and grow only logarithmically with  $k$  on small scales. The Newtonian-gauge CDM perturbation equals that in the comoving-gauge well inside the horizon, but on larger scales the Newtonian-gauge  $\Delta_c \approx -2\phi$  in matter domination.

For super-horizon modes, the dominant 21cm sources in the Newtonian gauge are

$$\delta f(\eta_A, \mathbf{x}_A, \epsilon, \hat{\mathbf{n}}) \approx \bar{f}(\epsilon) (\Delta_s + \psi) - \bar{f}_{\ln \epsilon}(\epsilon) \psi, \quad (32)$$

where we have ignored reionization. The source  $\Delta_s$  scales with the hydrogen perturbation  $\Delta_H$ . After recombination almost all the atoms are neutral and  $\Delta_H = \Delta_b$ . On scales above the baryon sound horizon at recombination the baryons fall into the CDM potential wells on a Hubble time scale, so  $\Delta_b$  evolves to follow  $\Delta_c$ . Note that although  $\Delta_b$  qualitatively follows  $\Delta_c$  well after recombination, the difference can be tens of percent on all sub-horizon scales at high redshift. On very small scales growth of  $\Delta_b$  is suppressed once the perturbation reaches pressure support. The Newtonian-gauge 21cm sources thus have a scale-invariant amplitude on super-horizon scales, scale as  $k^2$  for sub-horizon modes that entered the horizon after matter-radiation equality, are growing logarithmically on small scales, and are suppressed on very small scales where  $c_s^2 k^2/\mathcal{H}^2 \gtrsim 1$  at recombination. This behaviour can be seen in Fig. 3.

On small scales the fractional source fluctuation is of order of the CDM density perturbation,  $\Delta_s \sim (k/\mathcal{H})^2\phi$ , and the velocity  $v \sim (\mathcal{H}/k)\Delta_c$ . For small scales with  $k \gg \mathcal{H}$  the line-of-sight result in Eq. (22) is therefore dominated by the monopole and redshift distortions effects, giving the usual approximation for the 21cm source:

$$F_l(\eta_A, \mathbf{x}_A, \epsilon, k) \approx e^{-\tau_\epsilon} \bar{f}(\epsilon) \left[ \Delta_s j_l(k\chi_\epsilon) + \frac{kv}{\mathcal{H}} j_l''(k\chi_\epsilon) \right]. \quad (33)$$

One might expect the low- $l$  21cm fluctuations to be dominated by the super-horizon scale, post-Newtonian fluctuations at scale  $k = l/\chi$ . This is not correct since small-scale fluctuations, with amplitude growing rapidly with scale as  $k^2$ , do couple weakly to  $l < k\chi$  (through the oscillatory tails of the spherical Bessel functions). The net effect is that, for all  $l$  and a single source plane, the dominant contribution is from modes that are inside the horizon. At low  $l$ , the  $C_l$  integral of Eq. (23) is therefore dominated by much smaller scales, with  $k \gg l/\chi$ . In this limit the Bessel

functions can be approximated as  $j_l(k\chi) \sim \cos[k\chi - (l+1)\pi/2]/(k\chi)$ . Since the power spectrum is quite smooth we can then average over oscillations using  $\langle |j_l(k\chi)|^2 \rangle \sim 1/[2(k\chi)^2]$ . We can similarly remove oscillating terms in the second derivative term. Hence on large scales, keeping only the monopole source and redshift distortions and assuming a narrow redshift window, the dimensionless fractional power spectrum is

$$C_l(z, z) \sim 4\pi e^{-2\tau(z)} \int d \ln k \frac{\mathcal{P}_s(k; \eta_0 - \chi(z))}{2k^2 \chi(z)^2}, \quad (34)$$

where  $\mathcal{P}_s(k; \eta_0 - \chi(z))$  is the power spectrum of  $\Delta_s - kv/\mathcal{H}$  at redshift  $z$  (conformal distance  $\chi(z)$ ). Since this is independent of  $l$  it corresponds to a white noise spectrum. The intrinsic fluctuations on a scale  $k = l/\chi$  are hidden beneath random variations in the large scale distribution of much smaller perturbations. This is a generic feature of the 21cm angular power spectrum that is also true after the dark ages [5].

Scales inside the horizon at matter-radiation equality have an approximately scale-invariant spectrum (grow logarithmically with  $k$ ). This causes the 21cm power spectrum to flatten out. On scales where the wavelength is much smaller than the redshift bin width,  $l \gtrsim \chi/\Delta\chi$ , redshift distortion effects average out and we can use the Limber approximation:

$$C_l(z, z) \approx e^{-2\tau(z)} \frac{2\pi^2}{l^3} \int_0^{\chi_*} \chi d\chi W(\chi)^2 \mathcal{P}_{\Delta_s}(k = l/\chi(z); \eta_0 - \chi(z)), \quad (35)$$

where  $\mathcal{P}_{\Delta_s}$  is the power spectrum of the source  $\Delta_s$  and  $\chi_*$  is the far end of the window function  $W(\chi)$ . Since the source power spectrum is nearly scale invariant,  $C_l$  therefore scales approximately as  $1/l^3$ . In other words  $l^2 C_l$  is approximately constant with an additional  $1/l$  suppression due to line-of-sight averaging through the window. If  $W$  is a Gaussian of width  $\sigma$ , the line-of-sight averaging causes the overall amplitude to scale approximately as  $1/\sigma$ . The Limber approximation can in fact be used for numerical calculation on scales with  $l \gg \chi/\Delta\chi$  where it becomes accurate.

One very small scales where modes are inside the baryon sound horizon at recombination,  $kc_s(\eta_*)\eta_* \gtrsim 1$ , the baryon pressure becomes important and  $\Delta_H$  differs significantly from  $\Delta_c$  even at late times. We discuss approximate analytic solutions for the evolution of  $\Delta_b$  in Appendix A. In the small scale limit where  $k^2 c_s^2 \gg \mathcal{H}^2$  the pressure and gravitational forces approximately balance, and  $\Delta_b/\Delta_c \sim \mathcal{H}^2/(k^2 c_s^2)$ . Since  $\Delta_c$  is roughly scale invariant, and neglecting the effect of the baryon pressure on the CDM evolution, this implies  $l^2 C_l \propto 1/l^4$ , giving a characteristic sharp fall-off in power on very small scales (there is an additional power of  $1/l$  for window-function line-of-sight averaging). Note the observations on such small scales are unlikely to be possible at high redshift over most of the sky due to scattering by turbulent galactic and solar-system plasma [27].

## VI. NUMERICAL RESULTS

For our numerical results we assume a standard concordance flat adiabatic CDM ( $\Omega_c h^2 = 0.104$ ) model with a constant primordial spectral index ( $n_s = 0.95$ ) and optical depth to Thomson scattering  $\tau = 0.09$ . We take baryon density  $\Omega_b h^2 = 0.022$ , Hubble parameter  $73 \text{ km s}^{-1} \text{ Mpc}^{-1}$  and initial curvature perturbation power on  $0.05 \text{ Mpc}^{-1}$  scales  $A_s = 2.04 \times 10^{-9}$ . We neglect the neutrino masses, which do not have a large effect for sources planes at high enough redshift that the neutrinos are still relativistic. We take our window function to be a Gaussian of width  $\Delta\nu$  in frequency over the observed brightness.

In Fig. 4 we show the contribution of the auto-variance of various terms to the total power spectrum at a given redshift. As expected the dominant contributions are from the monopole source fluctuations and redshift distortions<sup>1</sup>. On small scales the next most important term is from the CMB dipole in the rest frame of the gas, which gives percent level contribution at  $l < 50$  for the redshift shown here, but is negligible on much smaller scales. At ( $l < 100$ ) the contribution from the potential and other velocity terms are also not entirely negligible. The contributions from the CMB temperature anisotropy above the dipole, and reionization re-scattering sources are completely negligible on all scales. At lower redshifts the background signal becomes smaller, and the relative importance of the terms changes. The background signal depends on  $\bar{T}_s - \bar{T}_\gamma$ , but some of the perturbation sources depend only on the 21cm optical depth and are non-zero even when the spin temperature is equal to the CMB temperature. As an extreme example, Fig. 5 shows the relatively large contribution from the photon-baryon dipole at  $z = 20$  on large scales if there were no additional sources from non-linear structures.

<sup>1</sup> Note that at the percent level it is important to use the baryon rather than CDM velocity when calculating the redshift distortions.

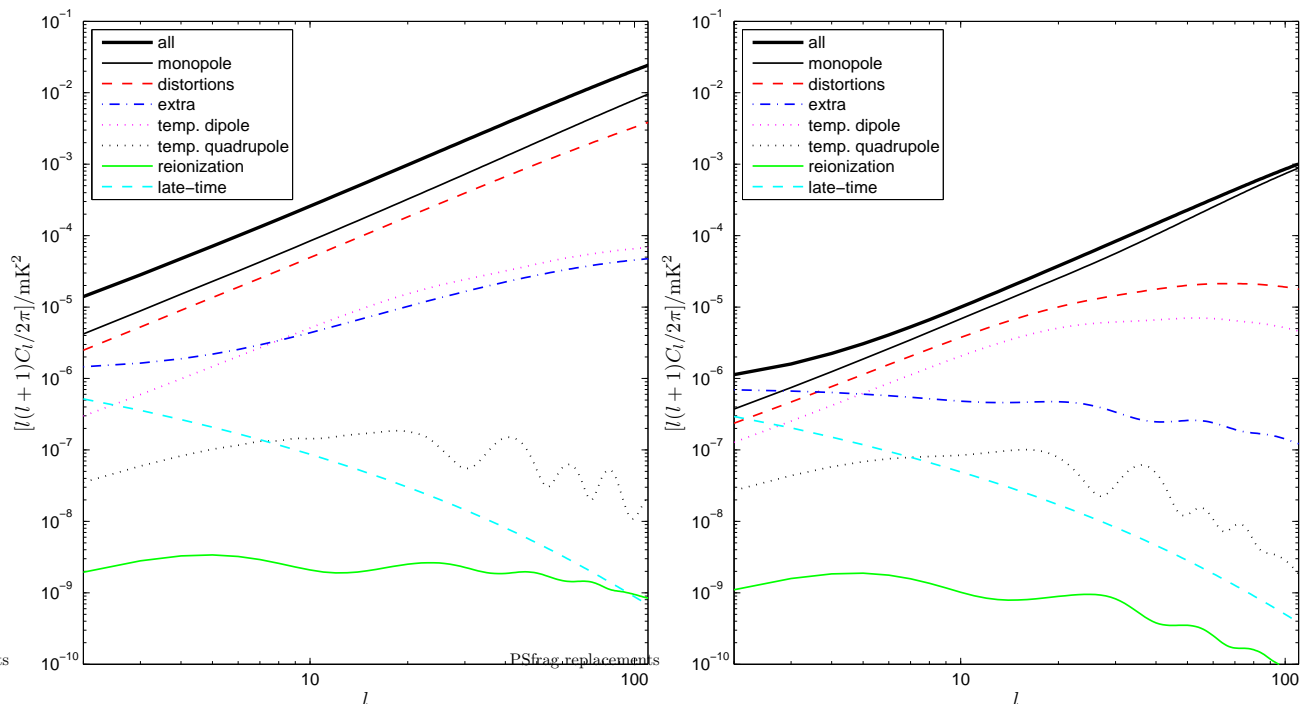


FIG. 4: Auto power spectra for the various terms in the 21cm power spectrum. Left: narrow window function at  $z = 50$  with  $\Delta\nu = 0.01\text{MHz}$  ( $T_b = -26\text{mK}$ ); Right: broad window function at  $z = 40$  with  $\Delta\nu = 5\text{MHz}$  ( $T_b = -15\text{mK}$ ,  $\sigma_z \sim 6$ ). Terms are calculated in the synchronous gauge, and ‘extra’ includes all effects not included in other curves; standard redshift distortions are defined here by the second term Eq. (33). The late-time curve is the ISW contribution from line-of-sight redshifting. The reionization curve is the result from sources at reionization, the other curves include the main  $e^{-2\tau}$  damping effect. The standard calculation includes only monopole and redshift distortion terms; the difference from the full result is  $\sim 1\%$  at  $l \lesssim 50$  growing to a few percent at low  $l$  for the narrow window function. For the broad window function that averages down small-scale power extra terms change the total by  $\gtrsim 1\%$  at  $l < 100$  (growing to  $\sim 40\%$  at low  $l$ ). Note that the total spectrum is not just the sum of the other autocorrelation terms since it also includes all cross-terms.

Note that just because something does not show up in a narrow frequency window auto-power spectrum at a given redshift does not mean that it is necessarily negligible. The correlation between source planes at a given  $l$  falls off very rapidly once the plane separation is greater than characteristic perturbation size  $\chi/l$ . Extra information may therefore be available in the cross-power spectra, particularly about small large-scale signals that are correlated between redshift bins. The effect of different frequency window functions is shown in Fig. 6. Here the baryon oscillations only show up when the window is wide enough to damp down the large smaller-scale fluctuations so that the power on baryon oscillation scales is not dominated by contributions from smaller scales. When narrow frequency windows are used this information is hidden in the cross-correlation structure of the different source planes.

The white-noise signal on large scales can be reduced by averaging over many redshift slices. Figure 4 shows the relative importance of the various scales on large scales when a broad redshift window function is used. Redshift distortions from scales smaller than the bin width are suppressed, and the large-scale white-noise monopole signal is reduced because of the line-of-sight averaging of small scale power. The relative importance of the additional terms is therefore larger. This raises the question of whether the large-scale 21cm signal can be useful, for example to learn about large scale power or as a source for the integrated Sachs-Wolfe effect<sup>2</sup> (ISW). There are two main problems. Firstly, a very broad window function is required to make the extra terms comparable to the monopole source, and residual monopole and redshift distortion signals will generally dominate. Secondly, since the dark age redshift shells are  $\gtrsim 3/4$  of the comoving distance to the last scattering surface, large-angle correlations, such as those due to Sachs-Wolfe potential redshifting, will be strongly correlated between redshift slices and correlated with the large-scale CMB. As an averaged source plane for the ISW the 21cm signal therefore has at least as much large-scale

<sup>2</sup> We thank Jeff Peterson for raising this question during a talk.

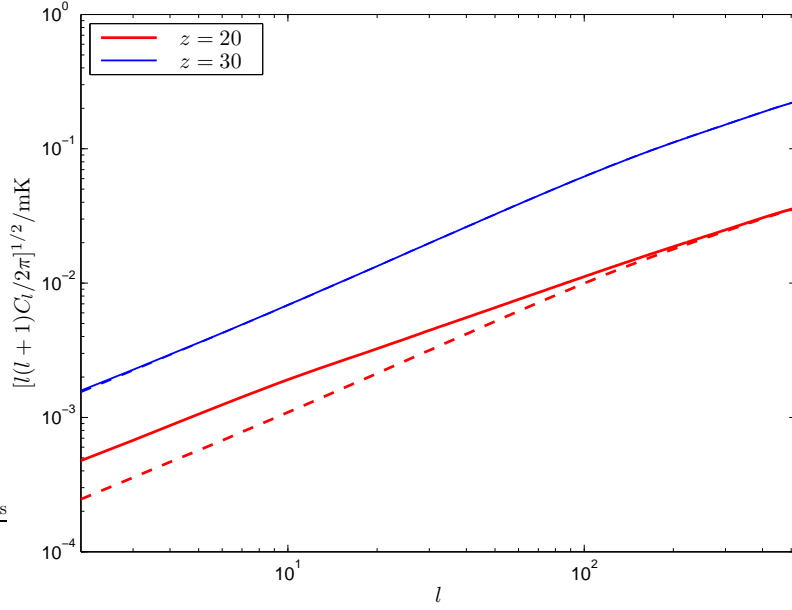


FIG. 5: The large-scale 21cm power spectrum at  $z = 20$  and  $z = 30$  if there were no Lyman- $\alpha$  sources or other non-linear effects ( $\Delta\nu = 0.01\text{MHz}$ ). Solid lines are the full linear result, dashed lines include only monopole and redshift-distortion sources. The difference is dominated by the baryon-photon velocity term.

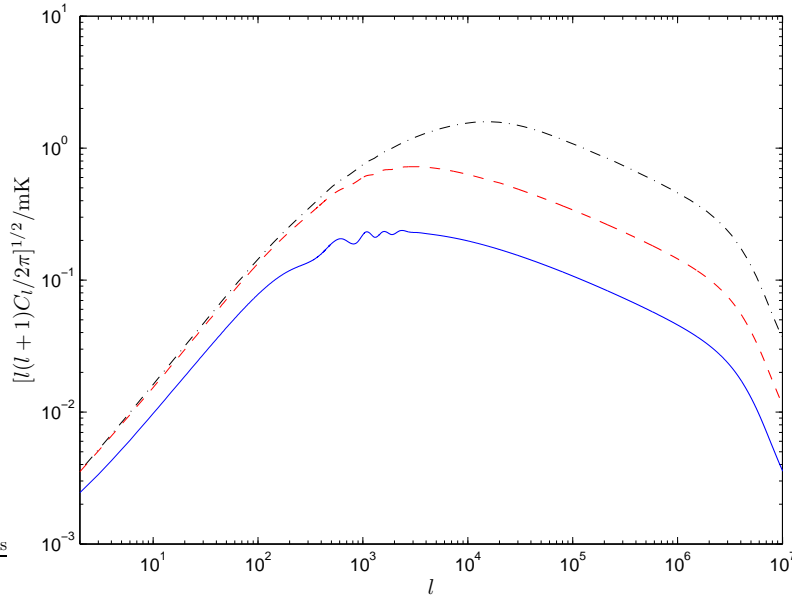


FIG. 6: The 21cm power spectrum at  $z = 50$  for  $\Delta\nu = \{1, 0.1, 0.01\}\text{MHz}$  (bottom to top). Large widths suppress the redshift-distortion contribution and allow the baryon oscillations to be seen. All show characteristic damping due to line-of-sight averaging over the bin width at  $l \gtrsim \chi/\Delta\chi$ , and the effect of baryon pressure at  $l \gtrsim 5 \times 10^6$ .

‘noise’ from other sources as the CMB and hence offers little extra information.

Decorrelation with source plane separation is a powerful way to try and separate intrinsic and foreground signals due to the much smoother signal (as a function of frequency) expected from most foregrounds [6, 28]. Detection of small non-foreground cross-correlations is therefore particularly challenging.

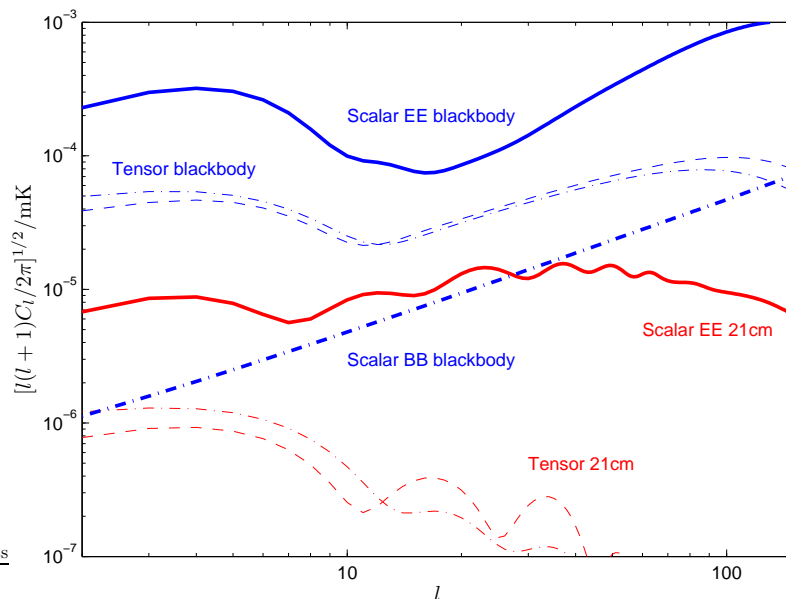


FIG. 7: The 21cm polarization power spectra from  $z = 50$  with  $\Delta\nu = 0.01\text{MHz}$ . Thick lines show the adiabatic scalar-mode signal, thin lines from  $r \equiv A_T/A_s = 0.1$  scale-invariant tensor modes. For comparison, the intrinsic CMB polarization signals (labelled blackbody) are also plotted: the scalar  $EE$  blackbody curve is the lensed E-mode polarization from scalar modes and the scalar  $BB$  blackbody curve is the lens-induced B-mode power; the tensor blackbody curves are the CMB polarization power spectra from gravity waves. For both intrinsic CMB and 21cm fluctuations, E-mode polarization is shown with solid or dashed lines and B-modes with dash-dotted lines. There are no 21cm scalar B-modes within our approximations. Reionization is assumed to be fairly sharp with optical depth  $\tau = 0.09$  ( $z_{\text{re}} \sim 12$ ).

## VII. POLARIZATION

A quadrupole anisotropy in the 21cm signal at reionization can generate polarization by Thomson scattering [29]. The signal is expected to be very small, but perhaps worth considering as polarization may be very useful to help with foreground cleaning of scalar modes. In principle the tensor mode signal can also be used as a cross-check on CMB temperature and polarization constraints on models of inflation.

Following standard methods [30, 31] it is straightforward to modify our scalar equations to include polarization in order to calculate the E-mode (gradient-like) spectrum generated at reionization. For our idealized analysis we neglect any effects due to magnetic fields, anisotropy of the hydrogen triplet state distribution and inhomogeneity of reionization. Typical numerical results are shown in Fig. 7.

Gravitational waves (tensor modes) are known to be subdominant to the scalar modes, but can also source anisotropies by their anisotropic shearing. There are two mechanisms. Firstly, the metric shear can directly change the 21cm photon frequency along the line of sight, which distorts the emission shell in much the same way as the redshift distortions and line-of-sight effects do for the scale modes. Secondly, the CMB temperature at absorption will be anisotropic due to gravitational waves between the absorber and the last scattering surface: this causes an anisotropy in the 21cm absorption. At reionization the quadrupole component of these anisotropies source both E and B polarization. The signal is a small fraction of the blackbody tensor signal because the optical depth for 21cm emission is only  $\sim 0.02$ . Note that since there is no intrinsic 21cm polarization before reionization the lensing-induced 21cm B modes are much smaller.

## VIII. LENSING

The line emission spectrum is not affected by lensing at first order. However perturbations along the line of sight can produce a non-negligible higher-order effect. The effect on the two- and three-dimensional power spectra has been analysed in detail in Ref. [32]. Lensing acts rather like a convolution of the angular power spectrum with the deflection-angle power spectrum. Since the 21cm power spectrum is rather smooth, the effect is significantly smaller than on the CMB. Nonetheless the baryon wiggles can be smoothed at well above the cosmic variance level. Here we

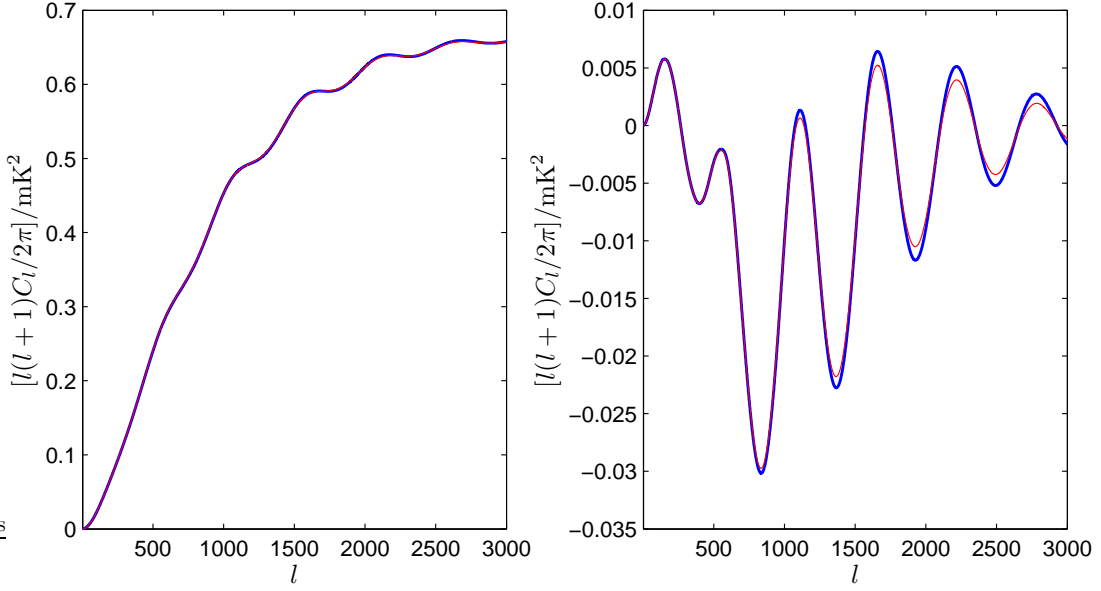


FIG. 8: The 21cm power spectrum for bins at  $z = 50$  and  $z = 52$  ( $\Delta\nu = 0.1\text{MHz}$ ), with lensing (thin lines) and without lensing (thick lines). The left figure shows  $C_l(z, z)$ , the right figure shows the small but non-negligible cross-correlation.

note a simple, non-perturbative approach to calculating the effect on the angular power spectrum. This is based on the lensed correlation function method often applied to the CMB temperature and polarization [33, 34, 35].

Since the lensing field is nearly linear the effect is well described in terms of the lensing deflection angle power spectrum  $C_l^\alpha(z, z')$ . In linear theory this is given in terms of the primordial power spectrum  $\mathcal{P}_{\mathcal{R}}(k)$  and transfer functions  $T_\Psi(k; \eta)$  for the Weyl potential,  $\Psi \equiv (\phi + \psi)/2$ , by (see e.g. Ref. [35])

$$C_l^\alpha(z, z') = 16\pi l(l+1) \times \int \frac{dk}{k} \mathcal{P}_{\mathcal{R}}(k) \left[ \int_0^{\chi(z)} d\chi T_\Psi(k; \eta_0 - \chi) j_l(k\chi) \left( \frac{\chi(z) - \chi}{\chi(z)\chi} \right) \right] \left[ \int_0^{\chi(z')} d\chi' T_\Psi(k; \eta_0 - \chi') j_l(k\chi') \left( \frac{\chi(z') - \chi'}{\chi(z')\chi'} \right) \right], \quad (36)$$

where  $\chi(z)$  is the conformal distance to the window at redshift  $z$ . We assume the window function is narrow compared to the distance so that the lensed sources can be approximated as a single source plane. For nearby bins the terms in square brackets are approximately equal.

In terms of  $C_l^\alpha(z, z')$  and the unlensed spectrum  $C_l(z, z')$ , the lensed power spectrum is given to very good accuracy by [35]

$$\tilde{C}_l(z, z') \approx \sum_l \frac{2l+1}{2} C_l(z, z') \int_{-1}^1 d\cos\beta d_{00}^l(\beta) e^{-l(l+1)\sigma^2(\beta)/2} \sum_{n=-l}^l I_n [l(l+1)C_{\text{gl},2}(\beta)/2] d_{n-n}^l(\beta), \quad (37)$$

where  $I_n$  is a modified Bessel function,  $d_{mn}^l$  are reduced Wigner functions,  $\sigma^2(\beta) \equiv C_{\text{gl}}(0) - C_{\text{gl}}(\beta)$ , and

$$C_{\text{gl},2}(\beta) \equiv \sum_l \frac{2l+1}{4\pi} C_l^\alpha(z, z') d_{-11}^l(\beta),$$

$$C_{\text{gl}}(\beta) \equiv \sum_l \frac{2l+1}{4\pi} C_l^\alpha(z, z') d_{11}^l(\beta). \quad (38)$$

The sum over  $n$  is dominated by the lowest terms with  $|n| \approx 0$ . For a  $\Delta\nu = 1\text{MHz}$  window at  $z = 50$ , the lensing-induced smoothing of the baryon oscillations can be nearly a percent, but elsewhere the effect on the angular power spectrum is generally very small because it is smooth on the scale of the width of the deflection angle power spectrum ( $\Delta l \sim 100$ ). Figure 8 shows the significant smoothing effect on the cross-correlation power spectrum on the scale of the baryon oscillations.

In addition to the small effect on the power spectrum calculated here and in Ref. [32], lensing also makes the distribution non-Gaussian. Combined with tomographic information this can be used for lensing reconstruction [36].

## IX. CONCLUSIONS

The 21cm signal from the dark ages is potentially a powerful probe of cosmology. We have derived full linear-theory results for the angular power spectra, and confirmed that, for most purposes, standard approximations including only monopole sources and redshift distortions are rather accurate. However additional velocity and potential terms can be non-negligible on very large scales, and our analysis allows for an accurate quantification of the error from neglecting these effects. In this paper we have focussed on theoretical issues. The observational problems are formidable, requiring many square-kilometers of collection area, low radio-noise, and, for high redshifts, getting outside the atmosphere to avoid the opaque ionosphere; see Refs. [3, 4, 6, 37] for further discussion. The additional hurdles to measure the distinctive polarization signal that we calculated, which is below the intrinsic blackbody signal, are quite possibly insurmountable.

Note that the 21cm spectrum is much more sensitive to the residual ionization fraction after recombination than the CMB temperature: the ionization fraction governs the evolution of the matter temperature which in turn affects the background brightness and the evolution of the perturbations. Current modelling of recombination is probably insufficiently detailed to be able to compute the 21cm power spectrum to an accuracy of more than a couple of percent as there are a wealth of subtle effects that need to be modelled to calculate hydrogen recombination accurately [38]. As an example of current uncertainties, using the result of Ref. [39] rather than RECFAST [20] for the post-recombination ionization fraction changes the 21cm brightness temperature at the two-percent level. If future observations are to achieve the  $\sim 10^{-5}$  constraints on cosmological parameters that are possible in principle, a very detailed analysis will be required of the full electron, atomic state and velocity distributions, with all interactions, extending the work of Ref. [17]. Furthermore, even at redshift of 50 the Jeans'-scale density perturbations are already  $\mathcal{O}(0.1)$  suggesting that non-linear corrections may be important at the sub-percent level, though these should be accurately calculable with a perturbative analysis (see e.g. Ref. [40]). However the additional post-Newtonian and velocity effects calculated in this paper are only important on large scales where precision is limited by cosmic variance, so the present work is largely complementary to these future challenges.

Although we have concentrated on the linear-theory power spectrum from the dark ages, much of our formalism can be adapted straightforwardly to the reionization epoch given models for the additional sources. Our numerical code is publicly available<sup>3</sup>.

## X. ACKNOWLEDGEMENTS

AL acknowledges a PPARC Advanced fellowship and AC a Royal Society University Research Fellowship. AL thanks Oliver Zahn, Steven Gratton and Jeff Peterson for discussion.

## APPENDIX A: BARYON PERTURBATION EVOLUTION

After recombination, Compton scattering has no significant effect on the baryon density evolution and the fractional synchronous gauge baryon perturbation  $\Delta_b$  obeys the equation

$$\begin{aligned} \frac{\partial^2 \Delta_b}{\partial \eta^2} + \mathcal{H} \frac{\partial \Delta_b}{\partial \eta} + k^2 c_s^2 \Delta_b &= 4\pi G a^2 \sum_i (\delta \rho_i + 3\delta p_i) \\ &\approx \frac{3}{2} \mathcal{H}^2 \Delta_m, \end{aligned} \tag{A1}$$

where  $(\rho_b + \rho_c)\Delta_m = \rho_c\Delta_c + \rho_b\Delta_b$  and the second line assumes matter domination. We make the approximation that  $\rho_c \gg \rho_b$  so the baryons have no effect on the CDM evolution and we can use the usual result in matter domination that  $\Delta_m(\eta) = \Delta_c(\eta) = \Delta_c(\eta_*)\eta^2/\eta_*^2$ . On small scales before recombination the baryons are tightly coupled to the photons and silk damping erases perturbations so that at recombination ( $\eta \sim \eta_*$ ) we have  $\Delta_b(\eta_*) \sim 0$  and  $\dot{\Delta}_b(\eta_*) \sim 0$ . On scales where baryon pressure is irrelevant,  $kc_s/\mathcal{H} \ll 1$  at all times, the solution after recombination is

$$\Delta_b/\Delta_c = 1 - 3 \left( \frac{\eta_*}{\eta} \right)^2 + 2 \left( \frac{\eta_*}{\eta} \right)^3. \tag{A2}$$

---

<sup>3</sup> <http://camb.info/sources>

On smaller scale the baryon pressure is important via the  $k^2 c_s^2$  term in Eq. (A1). The sound speed decays approximately as  $1/\eta$  while Compton scattering couples the gas temperature to the CMB temperature. Once coupling becomes ineffective at  $\eta \sim \eta_a$  the gas cools adiabatically and  $c_s$  decays as  $1/\eta^2$ . We can solve analytically for the evolution of the baryon perturbation for both limiting behaviours of the sound speed. For  $\eta_* < \eta < \eta_a$  the result is

$$\Delta_b/\Delta_c = \frac{6}{x^2 + 6} \left[ 1 - \left( \frac{\eta_*}{\eta} \right)^{5/2} \left( \cos[\sqrt{x^2 - 1/4} \ln(\eta/\eta_*)] + \frac{5}{2\sqrt{x^2 - 1/4}} \sin[\sqrt{x^2 - 1/4} \ln(\eta/\eta_*)] \right) \right], \quad (\text{A3})$$

where we defined  $x \equiv kc_s(\eta_*)\eta_*$  and assumed  $x > 1/2$ . The analytic continuation of this result to  $x = 0$  agrees with Eq. (A2). On large scales where modes are outside the baryon sound horizon at recombination ( $x \ll 1$ ) the perturbations fall into the CDM potential wells in the order of a Hubble time and  $\Delta_b \rightarrow \Delta_c$ . On small scales the baryon pressure causes the perturbations to oscillate once they reach pressure support. The relative amplitude of the oscillations about the midpoint decays as  $(\eta_*/\eta)^{5/2}$ , so by the time of adiabatic cooling we may neglect this term to  $\sim 10\%$  accuracy. The adiabatic cooling equation is a forced harmonic oscillator equation in  $1/\eta$  with solution involving sine and cosine integrals that can be written (for  $\eta > \eta_a$ ) as [41]

$$\Delta_b = A \cos(u) + B \sin(u) + \Delta_c \left[ 1 - u^2 \int_0^\infty dt \frac{te^{-ut}}{t^2 + 1} \right], \quad (\text{A4})$$

where  $u \equiv x\eta_a/\eta = kc_s(\eta)\eta$  and constants  $A$  and  $B$  are defined by the initial conditions. The term in square brackets monotonically decreases from one as  $k$  (and hence  $u$ ) increases, and describes the main effect of the pressure. Smoothly matching to Eq. (A3) (with the oscillation dropped) assuming a sharp transition at  $\eta_a$ , the result can be written as

$$\Delta_b/\Delta_c = 1 - u^2 \int_0^{x-u} \frac{\cos t}{t+u} dt - \frac{u^2}{6+x^2} \left( \cos(u-x) + \frac{4+x^2}{x} \sin(u-x) \right). \quad (\text{A5})$$

As a function of  $k$  this solution reproduces the qualitative fall-off in power show in Fig. 3, though the decaying nature of the solution is well hidden in Eq. (A5). The small-scale asymptotic form for  $k \rightarrow \infty$  ( $u, x \gg 1$ ) is

$$\Delta_b/\Delta_c = \frac{6}{u^2} - 12 \frac{u^2}{x^5} \sin(x-u) + \dots \quad (\text{A6})$$

$$= \frac{6}{[kc_s(\eta)\eta]^2} \left[ 1 - \mathcal{O}\left(\frac{1}{x} \frac{\eta_a^4}{\eta^4}\right) \right]. \quad (\text{A7})$$

As expected the transfer function falls off as  $\sim \mathcal{H}^2/(k^2 c_s^2)|_\epsilon$  on small scales with suppressed oscillations. This power-law fall off will only hold on scales where baryon diffusion can be neglected; on ultra-small scales the spectrum will be exponentially damped. Baryon pressure becomes important at  $k_{\text{pressure}} \sim 1/(c_s(\eta_*)\eta_*)$ , diffusion damping will become important at  $k_{\text{diffusion}} \sim k_{\text{pressure}}(\eta/\eta_{\text{coll}})_{\text{min}}^{1/2}$  where  $\eta_{\text{coll}}$  is the atomic collision time, which is always much smaller than  $\eta$  (see Fig. 1).

At redshifts of 30 to 100 residual Compton coupling actually gives  $c_s$  scaling as  $\eta^{-1.9}$  to  $\eta^{-1.6}$ , and approximating the transition in cooling behaviour as sharp may be expected to be a poor approximation on scales such that  $kc_s(\eta_a)\eta_a \gg 1$ . In this limit, the following approximation can be used:

$$\Delta_b(\eta)/\Delta_c(\eta) = \frac{6}{\eta^3} \int_{\eta_*}^{\eta} \frac{\eta'}{k\sqrt{c_s(\eta)c_s(\eta')}} \sin\left(\int_{\eta'}^{\eta} kc_s(\eta'') d\eta''\right) d\eta'. \quad (\text{A8})$$

This is derived from the WKB solutions of the homogeneous equation with Greens method. It is an exact solution for all  $k$  when the gas is adiabatically cooling, but only holds for  $kc_s(\eta_*)\eta_* \gg 1$  when Compton heating is still important. It can be shown that this result agrees with Eqs. (A3) and (A5) in the limit  $x \gg 1$  (and for a sharp transition to adiabatic cooling).

## APPENDIX B: GENERAL GAUGE AND NUMERICAL CALCULATION

We perform numerical calculations in the synchronous gauge. For convenience we give the equations in a general gauge here. The multipole equations in the 1+3 conventions of Refs. [42, 43] are

$$\begin{aligned} \dot{F}_l + \frac{k}{2l+1} [(l+1)F_{l+1} - lF_{l-1}] + \left[ \delta_{2l} \frac{2}{15} k\sigma - \delta_{0l} \dot{h} - \delta_{1l} \frac{1}{3} kA \right] \epsilon \partial_\epsilon \bar{f} \\ = a\bar{\rho}_s \delta(\epsilon/a - E_{21}) \left[ \delta_{l0} (\Delta_s - A) - \frac{T_\gamma}{T_s - T_\gamma} \left\{ \frac{\delta_{l1}}{3} (v_\gamma - v) + \sum_{\nu=2}^{\infty} \delta_{l\nu} \Theta_\nu \right\} \right] \\ - \frac{\delta_{l1}}{3} a\bar{\rho}_s v \partial_\epsilon [\epsilon \delta(\epsilon/a - E_{21})] - \dot{\tau} \left[ (\delta_{l0} - 1)F_l - \frac{\delta_{l1}}{3} v \epsilon \partial_\epsilon \bar{f} + \delta_{l2} \frac{F_2}{10} \right]. \end{aligned} \quad (\text{B1})$$

In the Newtonian gauge the acceleration  $A = -\psi$ , the scale factor perturbation  $h = -\phi$ , and the shear  $\sigma = 0$ . In the synchronous gauge  $A = 0$ ,  $h = h_s/6$  and the shear  $\sigma = (\dot{h}_s + 6\dot{\eta}_s)/2k$ , where  $h_s$  and  $\eta_s$  are the usual synchronous gauge quantities. Equation (B1) is valid in a general gauge but the individual terms are not gauge-invariant. In particular, under a change of velocity field,  $u^a \mapsto u^a + w^a$ , the multipoles transform as

$$F_0 \mapsto F_0 - \frac{w}{k} \left[ \dot{f} + \mathcal{H} \epsilon \partial_\epsilon \bar{f} \right] \quad (\text{B2})$$

$$\tilde{F}_1 \mapsto F_1 + \frac{1}{3} w \epsilon \partial_\epsilon \bar{f} \quad (\text{B3})$$

$$\tilde{F}_l \mapsto F_l \quad (l > 1). \quad (\text{B4})$$

For completeness, the other variables in Eq. (B1) transform as

$$\dot{h} \mapsto \dot{h} - \frac{1}{k} (\dot{w}\mathcal{H} + w\dot{\mathcal{H}}) + \frac{1}{3} kw, \quad (\text{B5})$$

$$\sigma \mapsto \sigma + w, \quad (\text{B6})$$

$$A \mapsto A + \frac{\dot{w}}{k} + \frac{\mathcal{H}w}{k}, \quad (\text{B7})$$

$$\Delta_s \mapsto \Delta_s - \frac{\dot{\rho}_s}{\rho_s} \frac{w}{k}, \quad (\text{B8})$$

$$v \mapsto v - w. \quad (\text{B9})$$

With these relations, one can establish the gauge-independence of Eq. (B1).

The line-of-sight solution is

$$\begin{aligned} F_l = \int d\eta e^{-\tau} \left\{ \left[ a\bar{\rho}_s (\Delta_s - A) \delta(\epsilon/a - E_{21}) + \dot{h} \epsilon \partial_\epsilon \bar{f} - \dot{\tau} F_0 \right] j_l(k\chi) + (kA - \dot{\tau}v) \epsilon \partial_\epsilon \bar{f} j_l'(k\chi) \right. \\ \left. - \left( \frac{k\sigma}{3} \epsilon \partial_\epsilon \bar{f} + \dot{\tau} \frac{F_2}{4} \right) [3j_l''(k\chi) + j_l(k\chi)] - a\bar{\rho}_s \left[ \partial_\epsilon [\epsilon \delta(\epsilon/a - E_{21})] v - \frac{\bar{T}_\gamma}{T_s - T_\gamma} (v - v_\gamma) \delta(\epsilon/a - E_{21}) \right] j_l'(k\chi) \right. \\ \left. - a\bar{\rho}_s \delta(\epsilon/a - E_{21}) \frac{\bar{T}_\gamma}{T_s - T_\gamma} \sum_{\nu=2}^{\infty} (2\nu + 1) \Theta_\nu i^\nu P_\nu \left( -\frac{i}{k} \frac{d}{d\chi_\epsilon} \right) j_l(k\chi) \right\} \end{aligned} \quad (\text{B10})$$

(for  $l > 1$ ), and the gas temperature perturbations evolve with

$$\dot{\Delta}_{T_g} = -\frac{2}{3} kv - 2\dot{h} - \frac{8a\sigma_T \bar{\rho}_\gamma x_e}{3m_e c(1 + f_{\text{He}} + x_e)} \left[ \left( 1 - \frac{\bar{T}_\gamma}{T_g} \right) (4\Delta_{T_\gamma} - A) + \frac{\bar{T}_\gamma}{T_g} (\Delta_{T_g} - \Delta_{T_\gamma}) \right], \quad (\text{B11})$$

where we again neglected  $\Delta_{x_e}$  (and helium fraction perturbations). Equations (27) and (30) in the main text hold in any gauge.

We choose to work in the synchronous gauge, evaluating the line-of-sight solution integrated over a frequency window function. We use the synchronous gauge because this is stable for isocurvature mode evolution, and because conventional calculations invariably use the baryon (or CDM) power spectrum in the synchronous gauge as outputted by CMBFAST or CAMB.

We define a window function  $W_f(\epsilon)$  so that we observe  $\int d\epsilon W_f(\epsilon)f$ . Then integrating over energies we use the functions

$$G(\eta) \equiv \int d\epsilon W_f(\epsilon) a \bar{\rho}_s \delta(\epsilon/a - E_{21}) = a^2 \bar{\rho}_s W_f(\epsilon_\eta) \quad (\text{B12})$$

$$V(\eta) \equiv \int d\epsilon W_f(\epsilon) \epsilon \partial_\epsilon \bar{f} = -\frac{a^2 \bar{\rho}_s}{\mathcal{H}} W_f(\epsilon_\eta) + \int^\eta d\eta' a(\eta') \frac{\partial}{\partial \eta'} \left( \frac{a(\eta') \bar{\rho}_s(\eta')}{\mathcal{H}(\eta')} \right) W_f(\epsilon_{\eta'}) \quad (\text{B13})$$

where  $W_f(\epsilon) = -W_f(z)E_{21}/\epsilon^2 = W_f(a)/E_{21}$ . For 21cm we assume we measure some averaged brightness temperature

$$\bar{T}_b = \int d\nu W_T(\nu) T_b(\nu). \quad (\text{B14})$$

Then

$$\bar{T}_b = \int da W_T(a) \frac{ch_p^3}{2k_B} \epsilon f \quad (\text{B15})$$

where  $W_T(a)$  is a window over dimensionless frequency, so

$$W_f(\epsilon) = \frac{ch_p^3}{2k_B} a W_T(a). \quad (\text{B16})$$

- 
- [1] D. Scott and M. J. Rees, *Mon. Not. Roy. Astron. Soc.* **247**, 510 (1990), ADS.
  - [2] A. Loeb and M. Zaldarriaga, *Phys. Rev. Lett.* **92**, 211301 (2004), astro-ph/0312134.
  - [3] S. Furlanetto, S. P. Oh, and F. Briggs, *Phys. Rept.* **433**, 181 (2006), astro-ph/0608032.
  - [4] C. L. Carilli, J. N. Hewitt, and A. Loeb (2007), astro-ph/0702070.
  - [5] R. Barkana and A. Loeb, *Astrophys. J.* **624**, L65 (2005), astro-ph/0409572.
  - [6] M. Zaldarriaga, S. R. Furlanetto, and L. Hernquist, *Astrophys. J.* **608**, 622 (2004), astro-ph/0311514.
  - [7] S. Bharadwaj and S. S. Ali, *Mon. Not. Roy. Astron. Soc.* **352**, 142 (2004), astro-ph/0401206.
  - [8] S. Naoz and R. Barkana, *Mon. Not. Roy. Astron. Soc.* **362**, 1047 (2005), astro-ph/0503196.
  - [9] R. Barkana and A. Loeb, *Mon. Not. Roy. Astron. Soc. Lett.* **363**, L36 (2005), astro-ph/0502083.
  - [10] C. Gordon and A. Lewis, *Phys. Rev.* **D67**, 123513 (2003), astro-ph/0212248.
  - [11] Y. A. Shchekinov and E. O. Vasiliev (2006), astro-ph/0604231.
  - [12] S. Furlanetto, S. P. Oh, and E. Pierpaoli, *Phys. Rev.* **D74**, 103502 (2006), astro-ph/0608385.
  - [13] A. Cooray, *Physical Review Letters* **97**, 261301 (2006), astro-ph/0610257.
  - [14] M. Valdes, A. Ferrara, M. Mapelli, and E. Ripamonti (2007), astro-ph/0701301.
  - [15] R. Khatri and B. D. Wandelt (2007), astro-ph/0701752.
  - [16] A. Challinor and A. Lewis (2007), in preparation.
  - [17] C. M. Hirata and K. Sigurdson, *MNRAS* pp. 19+ (2007), astro-ph/0605071.
  - [18] J. P. Wild, *Astrophys. J.* **115**, 206 (1952), ADS.
  - [19] S. Furlanetto and M. Furlanetto (2007), astro-ph/0702487.
  - [20] S. Seager, D. D. Sasselov, and D. Scott, *Astrophys. J. Suppl.* **128**, 407 (2000), astro-ph/9912182.
  - [21] R. Weymann, *Phys. Fluids* **8**, 2112 (1965).
  - [22] A. Loeb and M. Zaldarriaga, *Phys. Rev.* **D71**, 103520 (2005), astro-ph/0504112.
  - [23] C.-P. Ma and E. Bertschinger, *Astrophys. J.* **455**, 7 (1995), astro-ph/9506072.
  - [24] U. Seljak and M. Zaldarriaga, *Astrophys. J.* **469**, 437 (1996), astro-ph/9603033.
  - [25] W. Hu, U. Seljak, M. J. White, and M. Zaldarriaga, *Phys. Rev.* **D57**, 3290 (1998), astro-ph/9709066.
  - [26] A. Lewis, A. Challinor, and A. Lasenby, *Astrophys. J.* **538**, 473 (2000), astro-ph/9911177.
  - [27] B. J. Rickett, *ARAA* **28**, 561 (1990), ADS.
  - [28] K. K. Datta, T. R. Choudhury, and S. Bharadwaj (2006), astro-ph/0605546.
  - [29] D. Babich and A. Loeb, *Astrophys. J.* **635**, 1 (2005), astro-ph/0505358.
  - [30] W. Hu and M. White, *Phys. Rev.* **D56**, 596 (1997), astro-ph/9702170.
  - [31] A. Challinor, *Phys. Rev.* **D62**, 043004 (2000), astro-ph/9911481.
  - [32] K. S. Mandel and M. Zaldarriaga, *Astrophys. J.* **647**, 719 (2006), astro-ph/0512218.
  - [33] U. Seljak, *Astrophys. J.* **463**, 1 (1996), astro-ph/9505109.
  - [34] A. Challinor and A. Lewis, *Phys. Rev.* **D71**, 103010 (2005), astro-ph/0502425.
  - [35] A. Lewis and A. Challinor, *Phys. Rept.* **429**, 1 (2006), astro-ph/0601594.

- [36] O. Zahn and M. Zaldarriaga (2005), astro-ph/0511547.
- [37] J. B. Peterson, K. Bandura, and U. L. Pen (2006), astro-ph/0606104.
- [38] E. R. Switzer and C. M. Hirata (2007), astro-ph/0702145.
- [39] J. A. Rubino-Martin, J. Chluba, and R. A. Sunyaev, *Mon. Not. Roy. Astron. Soc.* **371**, 1939 (2006), astro-ph/0607373.
- [40] B. Jain and E. Bertschinger, *Astrophys. J.* **431**, 495 (1994), astro-ph/9311070.
- [41] M. Abramowitz and I. A. Stegun, *Handbook of Mathematical Functions* (Handbook of Mathematical Functions, New York: Dover, 1972), ISBN 0486612724.
- [42] A. Challinor and A. Lasenby, *Astrophys. J.* **513**, 1 (1999), astro-ph/9804301.
- [43] A. Lewis and A. Challinor, *Phys. Rev.* **D66**, 023531 (2002), astro-ph/0203507.